Nanomedicine: Nanotechnology, Biology, and Medicine
19 (2019) 126–135

nanomedjournal.com

Subtle changes in surface-tethered groups on PEGylated DNA nanoparticles significantly influence gene transfection and cellular uptake

Xiyu Ke, PhD[a,b,1], Zonghui Wei, PhD[c,1], Ying Wang, PhD[a,b], Sabrina Shen, B.S.[a], Yong Ren, PhD[a,b], John-Michael Williford, PhD[b], Erik Luijten, PhD[d,e,f,*], Hai-Quan Mao, PhD[a,b,g,**]

[a]*Department of Materials Science and Engineering, Whiting School of Engineering, Johns Hopkins University, Baltimore, MD, United States*
[b]*Institute for NanoBioTechnology, Johns Hopkins University, Baltimore, MD, United States*
[c]*Graduate Program in Applied Physics, Northwestern University, Evanston, IL, United States*
[d]*Department of Materials Science and Engineering, Northwestern University, Evanston, IL, United States*
[e]*Department of Engineering Sciences and Applied Mathematics, Northwestern University, Evanston, IL, United States*
[f]*Department of Physics and Astronomy, Northwestern University, Evanston, IL, United States*
[g]*Translational Tissue Engineering Center and Department of Biomedical Engineering, Johns Hopkins School of Medicine, Baltimore, MD, United States*

Revised 3 April 2019

Abstract

PEGylation strategy has been widely used to enhance colloidal stability of polycation/DNA nanoparticles (NPs) for gene delivery. To investigate the effect of polyethylene glycol (PEG) terminal groups on the transfection properties of these NPs, we synthesized DNA NPs using PEG-*g*-linear polyethyleneimine (*l*PEI) with PEG terminal groups containing alkyl chains of various lengths with or without a hydroxyl terminal group. For both alkyl- and hydroxyalkyl-decorated NPs with PEG grafting densities of 1.5, 3, or 5% on *l*PEI, the highest levels of transfection and uptake were consistently achieved at intermediate alkyl chain lengths of 3 to 6 carbons, where the transfection efficiency is significantly higher than that of nonfunctionalized *l*PEI/DNA NPs. Molecular dynamics simulations revealed that both alkyl- and hydroxyalkyl-decorated NPs with intermediate alkyl chain length exhibited more rapid engulfment than NPs with shorter or longer alkyl chains. This study identifies a new parameter for the engineering design of PEGylated DNA NPs.

Key words: PEGylated DNA nanoparticles; PEG terminal group; Transfection; Cellular uptake; Molecular dynamics simulation

Various polycations, including polyethyleneimine (PEI), polyphosphoramidate, poly(β-amino ester), poly(L-lysine), *etc.*, have been used as non-viral gene vectors by forming nanoparticles (NPs) through charge-mediated complexation with nucleic acids.[1–3] Compared to viral vectors, polycations offer the advantage of low immunogenicity, high cargo loading capability, and ease of large-scale production.[1] Among these polycations, PEI is considered the gold standard, owing to its high transfection efficiency *in vitro*.[4] However, *in vivo* applications of PEI/DNA NPs have been hindered by low colloidal stability and toxicity to healthy tissues stemming from their high positive charge density.[4,5] To circumvent these limitations, polyethylene glycol (PEG)-modified PEI has been designed and synthesized in the form of either block copolymers or graft copolymers with PEG grafted on the PEI backbone.[6–10] Such PEGylated PEI is capable of complexation with DNA into

Conflict of Interest: Authors report no conflict of interest.

Acknowledgment: This work was supported by NIH/NIBIB grant R01 EB018358 (HQM and EL). We thank Ming Han for valuable discussions. We also acknowledge the Quest high-performance computing facility at Northwestern University for computational resources.

*Correspondence to: E. Luijten, Department of Materials Science and Engineering, Northwestern University, Evanston, IL, USA.
**Correspondence to: H.-Q. Mao, Institute for NanoBioTechnology, Johns Hopkins University, Baltimore, MD, USA.
E-mail addresses: luijten@northwestern.edu, (E. Luijten), hmao@jhu.edu. (H.-Q. Mao).
[1] Authors contributed equally.

https://doi.org/10.1016/j.nano.2019.04.004
1549-9634/

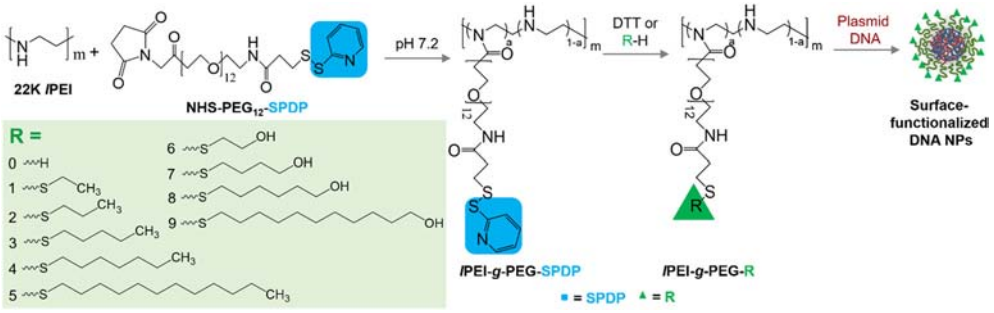

Figure 1. Preparation of PEGylated DNA NPs with various PEG terminal groups.

NPs with PEI/DNA in their core and PEG on the surface. The resulting particles have demonstrated enhanced colloidal stability, prolonged blood circulation time, and lower toxicity compared to PEI/DNA NPs.[6,11,12]

The introduction of PEG to polycation/DNA NPs greatly expands the parameter space that can be tuned to achieve higher gene delivery efficiency. Several studies have revealed that PEG length and grafting density significantly influence the properties and transfection efficiency of PEGylated PEI/DNA NPs.[6,7,13] For example, we previously studied DNA delivery using 22-kDa linear PEI (*l*PEI) grafted with different densities of 0.7-kDa or 2-kDa PEG chains.[6] Both NPs showed comparable colloidal stability, but those with 0.7-kDa PEG grafts exhibited significantly higher *in vitro* transfection efficiency in metastatic prostate PC3 cells than the NPs with 2-kDa PEG at different PEG grafting densities. Additionally, the transfection efficiency of both types of NPs decreased with increasing PEG grafting density. Whereas these findings are promising, few studies have explored extensions beyond pure PEG-modified polycations as gene carriers. Specifically, to our knowledge there are no published findings on the effect of PEG terminal groups on the biological activity of PEGylated DNA NPs. We observed that changing the PEG terminal groups of *l*PEI-*g*-PEG_{7H}/DNA NPs from methoxy to hydroxyl significantly enhanced their transfection efficiency (for PEG grafting densities between 0.2 and 2.3%) in PC3 cells as well as main organs (*e.g.,* lung, heart, and kidney) of Balb/c mice after intravenous (*i.v.*) injection.[14] This suggests that PEG terminal groups may play an important role in controlling the biological activity of PEGylated DNA NPs and that subtle changes in the PEG terminal groups affect the NP performance both *in vitro* and *in vivo*. Here, we aim for a systematic understanding of these effects, which can provide a cornerstone for the rational design of effective non-viral gene carriers.

We synthesized two series of NPs by mixing plasmid DNA and *l*PEI_{22K}-*g*-PEG_{5H}-R polymers with different PEG terminal groups (R) containing either alkyl chains (with n = 0, 2, 3, 5, 7, or 12 carbon atoms) or alkyl chains with hydroxyl terminal groups (with n = 2, 4, 6, or 11 carbon atoms) at different PEG grafting densities (0.5, 1.5, 3, 5, and 10%) (Figure 1). To investigate the effect of the terminal groups and the PEG surface densities on the biological activity of these surface-functionalized DNA NPs, we characterized particle size, size distribution, zeta potential, and heparin challenge stability. In addition, we studied their cytotoxicity, transfection, and cellular uptake efficiency in PC3 cells. Furthermore, we complemented this experimental work with molecular dynamics (MD) simulations to gain insight into the role played by alkyl chain length in determining the interactions between cell membranes and surface-functionalized NPs.

Methods

Additional details are found in the supplementary information (SI) section.

Functional group modification

Various small molecules with thiol group (R-H) were dissolved in methanol (1 mg/mL) and then added into 1 mL of *l*PEI-*g*-PEG-SPDP polymer solution to achieve a molar ratio of 10 to 1 (thiol group to SPDP group). The mixture solution was stirred overnight at room temperature. The conversion efficiency was determined by measuring the UV absorbance of 2-thione pyridine after conjugation. The efficiency for different small molecules was controlled to be around 100% by using sufficiently high feeding ratios of R-H to *l*PEI-*g*-PEG-SPDP. After reaction, the mixture solution was purified by ultracentrifugation using a dialysis tube with a MWCO of 3000 Da to obtain functionalized *l*PEI-*g*-PEG polymers with various PEG terminal groups.

Transfection efficiency assay

PC3 cells were seeded on a 96-wells plate at a cell density of 1×10^4 cells/well. After incubation for 24 h, the cell culture medium was replaced with serum-free DMEM containing DNA NPs (0.25 μg DNA/well). The cells were allowed to incubate for an additional 4 h, and then the DNA-containing medium was changed to fresh cell culture medium. The cells were incubated for another 44 h, and then lysed by Reporter Lysis Buffer (Promega, Madison, WI). The Luciferase expression level was measured using Luciferase Assay System kit (Promega, Madison, WI) following the manufacturer's protocol. The luminescence intensity was recorded using a SpectraMax i3x Multi-Mode microplate reader (Molecular Devices, Sunnyvale,

CA) and then normalized to the total protein content measured using bicinchoninic acid (BCA) assay (Pierce, Rockford, IL).[6]

Cellular uptake analysis

PC3 cells were seeded on a 24-well plate at a cell density of 5×10^4 cells/well. After incubation for 24 h, the cell culture medium was replaced with serum-free DMEM containing DNA NPs prepared using YOYO-1 labeled DNA (1.25 μg DNA/well). After further incubation for 4 h, the cells were washed three times by clod PBS and then incubated for 30 min with PBS containing 100 IU/mL heparin and 75 mmol/L sodium azide to remove any bound extracellular DNA NPs.[15] The cells were trypsinized and suspended in PBS to obtain a single-cell solution. Subsequently, they were analyzed using flow cytometry (BD FACSCalibur). The geometric mean fluorescence intensity of each sample was calculated based on signals collected from 5000 events and the data were analyzed using FlowJo software. Each sample was run in triplicate and the data are presented as mean ± standard deviation.

Modeling details

In our coarse-grained model, assemblies of spherical beads were employed to represent all molecules. The cell membrane was modeled as a bilayer of 4-bead-long lipids with one head bead and three tail beads. Each bead had a diameter σ, where σ is the Lennard–Jones (LJ) unit of length, which was set to 0.7 nm to yield an appropriate membrane thickness. 12,800 lipid molecules spanned the entire cross-section of the simulation box. Each PEGylated DNA NP was modeled as a combination of a rigid spherical core and a corona formed by modified PEG grafts directly bonded to the core. The core was composed of a central bead with a diameter of 20σ and 936 surface beads with diameter σ, as illustrated in Figure S1. The central bead was introduced to prevent any molecules from penetrating into the NP core. The PEG grafts were directly bonded to the surface beads and the PEG surface density was chosen according to the estimated experimental value, *i.e.*, a grafting density of 3%. In this estimation, we assumed that a typical NP contains 6 plasmid DNA molecules (with 6731 base pairs each) and has a diameter of approximately 100 nm.[16] At an experimental pH condition of around 7, the charge density of a *l*PEI backbone is close to 34%.[17] Therefore, each NP contained about 464 PEG-grafted *l*PEI, assuming the electroneutrality condition (the real NP are overcharged). Based on these assumptions, the surface area per PEG (chain length of 4.2 nm) was estimated to be around 4.5 nm^2 at a grafting density of 3%. In the simulations, the surface area per PEG was set to be around 3.2 nm^2 and each PEG chain was represented by 5 beads with a diameter of σ (corresponding to a total PEG length of 3.5 nm).

The beads in the lipids or modified PEG grafts were bonded *via* a harmonic potential,

$$U_{\text{bond}} = k(r-r_0)^2, \quad k = 30\, k_{\text{B}}\, T/\sigma^2,$$

where r is the center-to-center distance between two beads and $r_0 = 2^{1/6}\sigma$. An additional harmonic bond-angle potential was applied to each lipid to maintain a linear structure,

$$U_{\text{angle}} = k_\theta(\theta-\theta_0)^2, \quad k_\theta = 5\, k_{\text{B}}\, T,$$

where θ is the angle between two adjacent bonds and $\theta_0 = 180°$. In the implicit-solvent representation, we used LJ potentials to describe the pair interactions. All hydrophilic beads (*i.e.*, lipid heads, NP cores, PEG, and hydroxyl terminal groups) interacted *via* a purely repulsive LJ potential with strength $\varepsilon = 1.0\ k_{\text{B}}T$ and cutoff at $2^{1/6}\sigma$, shifted to eliminate the discontinuity at the cutoff. For the interactions between hydrophobic beads (*i.e.* lipid tails and alkyl chains), we employed a widely used generic lipid model to efficiently account for hydrophobicity.[18,19] Specifically, the hydrophobic beads experience an effective attraction,

$$U_{\cos}(r) = \begin{cases} 4\varepsilon\left((\sigma/r)^{12}-(\sigma/r)^{6}\right), & 0<r<2^{1/6}\sigma \\ -\varepsilon\cos^2\dfrac{\pi\left(r-2^{1/6}\sigma\right)}{2\times 1.4\sigma}, & 2^{1/6}\sigma \le r \le 2^{1/6}\sigma + 1.4\sigma \\ 0, & r>2^{1/6}\sigma + 1.4\sigma \end{cases}$$

where $\varepsilon = 1.0\ k_{\text{B}}T$. Electrostatic interactions are accounted for through Ewald summation.

The LAMMPS package was used to perform the MD simulations. In the studies of NP and cell membrane interactions, all system components were placed in a simulation box of size $93 \times 93 \times 80\sigma^3$ and the center of the NP was initially placed approximately 27σ above the center of the membrane. Periodic boundary conditions were applied in three dimensions. To allow reconfiguration of the membrane when interacting with the NP, we applied a Berendsen barostat to keep the system under a constant pressure equal to the osmotic pressure of the added salt solution. The x–y components and z component of the pressure tensor were varied independently, whereas the x and y components were coupled. The simulations were performed for at least 4×10^6 steps with a time step of 0.005τ, where τ is the LJ unit of time.

Results

Surface-functionalized DNA NPs preparation and characterizations

The *l*PEI-*g*-PEG-R polymers with different PEG grafting densities and terminal groups shown in Figure 1 were synthesized following our previously published protocol.[6] First, *l*PEI-*g*-PEG polymers with SPDP terminal groups (*i.e.*, *l*PEI-*g*-PEG-SPDP in Figure 1) were synthesized by grafting NHS-PEG-SPDP (MW 500 Da) onto *l*PEI (MW 22 kDa) through the reaction between the NHS group and the amine groups in *l*PEI. The structure of *l*PEI-*g*-PEG with SPDP terminal group has been confirmed using ^{1}H-NMR according to our previously reported protocol.[6] The PEG grafting density was determined by measuring the concentration of released by-product pyridine-2-thione at 343 nm after reacting SPDP-conjugated *l*PEI-*g*-PEG with DTT. The standard curve was generated simultaneously by reacting different concentrations of NHS-PEG-SPDP with excess amount of DTT using the same

assay (Figure S2). The resulting *l*PEI-*g*-PEG-SPDP polymers at PEG grafting densities of 0.5, 1.5, 3, 5, and 10% were conjugated with a library of small molecules with thiol groups (R-H in Figure 1) or dithiothreitol (DTT) to convert the SPDP groups to the desired PEG terminal groups. Lastly, *l*PEI-*g*-PEG-R/DNA NPs (labeled NP0 to NP9 according to the PEG terminal groups R in Figure 1) were prepared through rapid mixing of the polymer solution and g-Wiz luciferase plasmid DNA solution (50 μg/mL) at N/P ratio (ratio of nitrogen in *l*PEI-*g*-PEG-R to phosphorus in DNA) 8.

The particle size and size distribution of the NPs were measured *via* dynamic light scattering. NPs formed with polymers at PEG grafting densities of 0.5 to 5% display average particle sizes between 59 and 188 nm (Figure S3, *A*). Within this range of grafting densities, the terminal groups do not have a significant effect on particle size. However, the polydispersity index (PDI) of the NPs increases with increasing PEG grafting densities (Figure S3B). NPs formed with polymers at PEG grafting densities of 0.5 to 3% have PDI values ranging from 0.10 to 0.21, whereas at a PEG grafting density of 10%, large PDI values (0.26 to 1.0) indicate the presence of nonuniform DNA NPs. DNA NPs formed with unmodified *l*PEI have an average particle size of 72 nm and a PDI of 0.15. For all surface-functionalized NPs we found a positive surface charge, with zeta potentials ranging from +21 to +39 mV, compared to a zeta potential of +38 mV for *l*PEI/DNA NPs (Figure S4).

Stability assay

To determine NP stability, we challenged them with heparin solutions at various concentrations. The EC_{50} values, the heparin concentrations needed to achieve 50% DNA release, are summarized in Figure S5, *A*. Generally, the stability of NPs with PEG grafting densities of 1.5 and 3% was higher than of NPs with PEG grafting densities of 0.5, 5, and 10%. While the grafting density affected the stability of the NPs, all polymers showed similar DNA binding ability as *l*PEI at N/P ratio 8 (Figure S5, *B*).

Cytotoxicity assay

The cytotoxicity of PEGylated NPs was evaluated in human prostate cancer PC3 cells. After treatment with NPs at a PEG grafting density of 0.5%, the average metabolic activity of PC3 cells lay between 39 and 67%, compared to an activity of 55% for those treated with *l*PEI/DNA NPs (Figure S6). Interestingly, we observed improved cell viability with increasing PEG grafting density. At PEG grafting densities higher than 1.5%, most NPs showed a low toxicity, with cell viability higher than 80%. Generally, the cell viability first decreased and subsequently increased with increasing alkyl chain length.

Transfection assay

Having obtained this understanding of the properties and cytotoxicity of surface-functionalized DNA NPs, we characterized their transfection efficiency in PC3 cells as a function of terminal group and alkyl length (Figure 2). Unsurprisingly, at low grafting density PEG decoration had a negligible effect on the transfection activity of DNA NPs, as demonstrated by the results for different alkyl chain lengths (NP0 to NP5) at a PEG grafting density of 0.5%, which showed no significant differences from *l*PEI/DNA NPs. At higher PEG grafting densities, the transfection efficiency of the surface-functionalized NPs generally reached a maximum for NP2 ($R = CH_3(CH_2)_2S–$) and then decreased with increasing alkyl chain length. Most importantly, NP2 showed far higher transfection levels than *l*PEI/DNA NPs (3.2-, 6.0-, 9.4-, and 3.8-fold increase at grafting densities of 1.5, 3, 5, and 10%, respectively). Similarly, for hydroxyalkyl-terminated PEG (NP6 to NP9) at PEG grafting density 0.5%, all surface-functionalized NPs showed transfection levels comparable to *l*PEI/DNA NPs. At PEG grafting densities of 1.5 and 3%, we again observed a nonmonotonic trend of transfection efficiency as a function of alkyl chain length, with the highest transfection efficiency at NP8 ($R = HO(CH_2)_6S–$), namely a 6.3- and 14.8-fold increase compared to *l*PEI/DNA NPs at PEG grafting densities 1.5 and 3%. At even higher PEG grafting densities of 5 and 10%, all NPs showed transfection levels similar to or lower than *l*PEI/DNA NPs. The highest transfection levels of the two series of NPs were achieved for NP2 ($R = CH_3(CH_2)_2S–$) at PEG grafting density 5% and NP8 ($R = HO(CH_2)_6S–$) at PEG grafting density 3%.

Cellular uptake assay

The cellular uptake levels of various *l*PEI-*g*-PEG-R/DNA NPs were evaluated in PC3 cells using flow cytometry and correlated with the transfection efficiency. We found that most PEGylated NPs exhibited cellular uptake lower than or similar to *l*PEI/DNA NPs, except for NP2 at PEG grafting density 3% and NP8 at PEG grafting densities of 0.5, 1.5, and 3% (Figure 3). At all grafting densities, the cellular uptake levels varied non-monotonically with alkyl chain length, reaching their highest values for NP2 and NP8, without and with hydroxyalkyl groups, respectively. However, the variation in cellular uptake level differed from that found for the transfection efficiency. For instance, NP2 at a PEG grafting density of 10% showed much lower cellular uptake than *l*PEI/DNA NPs, whereas its transfection efficiency was significantly higher. This is illustrated in Figure 4, showing the transfection efficiency as a function of the cellular uptake level for different NPs and PEG grafting densities. At PEG grafting densities of 1.5, 3, and 5%, the cellular uptake levels were positively correlated with the transfection efficiency, but at 0.5 and 10% no clear correlations were observed.

Intracellular distribution

The flow cytometry results were confirmed by the intracellular distributions, observed *via* confocal microscopy, of free DNA, *l*PEI/DNA NPs, NP5, and NP8 at a PEG grafting density of 3%. Cells treated with *l*PEI/DNA NPs or NP8 indeed show much stronger fluorescence signals inside cells than those treated with free DNA or NP5 (Figure S7). Furthermore, strong DNA signals were found inside the nuclei of cells treated with NP8, in contrast to cells treated with *l*PEI/DNA NPs, for which the DNA was mostly located in the cytosols.

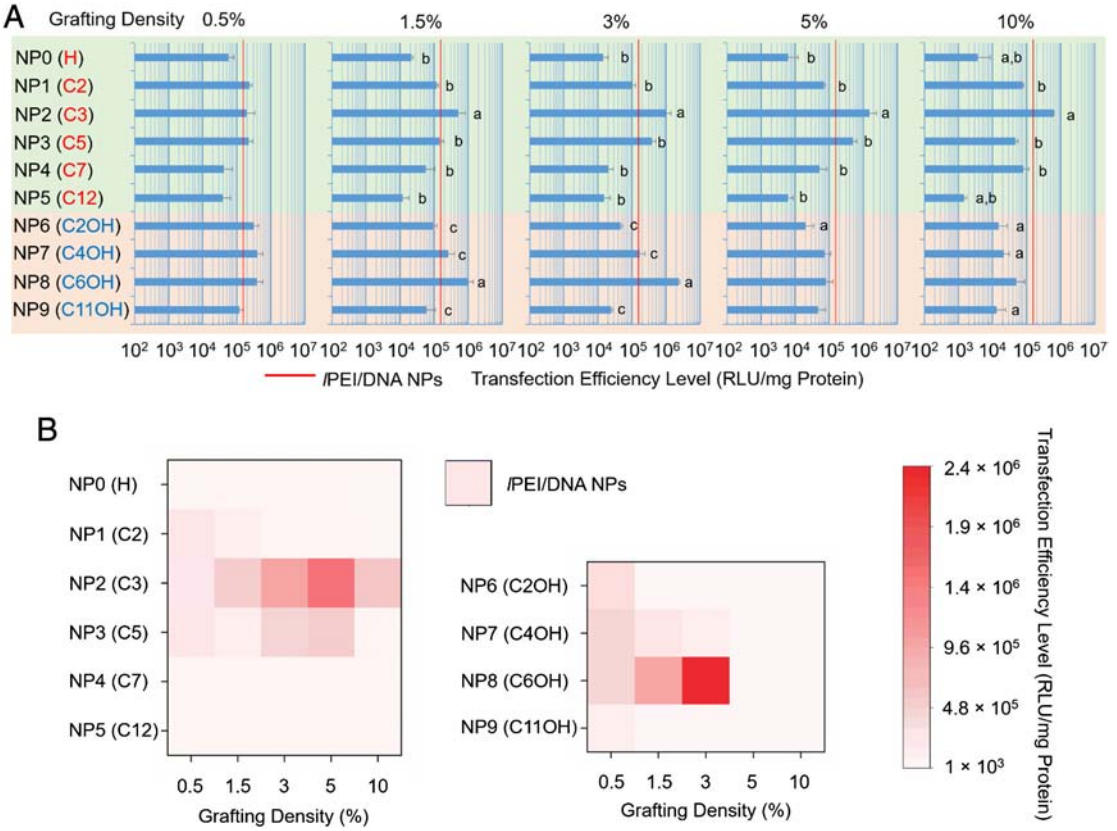

Figure 2. Transfection efficiency of PEGylated DNA NPs with different PEG terminal groups in PC3 cells. **(A)** Bar charts showing the transfection efficiency values of various NPs. Unmodified /PEI/DNA NPs are used as control, with their transfection values shown in red. a, $P < 0.05$, *vs.* /PEI/DNA NPs; b, $P < 0.05$, *vs.* NP2; c, $P < 0.05$, *vs.* NP8. **(B)** Heat maps comparing the transfection levels of various NPs.

MD simulation study

The interaction of surface-functionalized DNA NPs with cell membrane was further investigated using MD simulations. We first equilibrated the structure of the resulting surface-functionalized NP at a fixed distance above a pre-equilibrated membrane, along with the counterions to the NP and the membrane, as well as monovalent salt at ~10% of physiological concentration. Subsequently, we released the NP and monitor its interaction with the membrane. Figure 5 depicted the evolution of the system for various surface-functionalized NPs. In each case, $t = 0$ equals the time at which an alkyl chain bead first comes into contact with the membrane, defined as an alkyl chain bead separated by less than 0.98 nm from any hydrophobic lipid tail bead. For the alkyl-decorated NPs (Figure 5, *A*), the NP merely showed attachment to the membrane when the alkyl chain length is short (1 bead), but for alkyl chains of 2 beads the membrane gradually wrapped around the NP and reached a state with a large degree of engulfment at the end of the simulation. At longer alkyl chain length (3 or 4 beads), this wrapping process was still observed, but it proceeded at a slower rate than for a chain length of 2 beads. A similar nonmonotonic trend as a function of alkyl chain length was observed for the hydroxyalkyl-decorated NPs (Figure 5, *B*), with the threshold for engulfment shifted to a chain length of 3 hydrophobic beads. Figure 6 also showed that the NPs with intermediate alkyl chain length (2 beads for alkyl-decorated NPs and 3 beads for hydroxyalkyl-decorated NPs) had the highest percentage of hydrophobic beads interacted with the cell membrane over time.

Discussion

DNA delivery is a highly complex process affected by a range of factors. To accurately account for these parameters, we probed several important properties before characterizing the effect of PEG terminal groups on the transfection efficiency of surface-functionalized DNA NPs. Notably, particle size strongly correlates with cellular uptake of NPs, as particles smaller than 200 nm enter and accumulate in cells through clathrine-mediated endocytosis more efficiently than those around 500 nm.[20,21] NPs formed by polymers at PEG grafting densities lower than 10% showed particle size ranging from 59 to 188 nm (Figure S3, *A*), which is suitable for effective cellular uptake. In addition, NPs formed by polymers with low PEG grafting densities showed better uniformity than those formed by polymers with high PEG grafting densities (Figure S3, *B*). A probable explanation lies in the weakening of the electrostatic interactions between the polymers and DNA owing to the high grafting density of the PEG.

The stability of DNA NPs may also influence several steps of the delivery process, including blood circulation and cellular uptake.[22] The results showed that NPs formed by polymers at

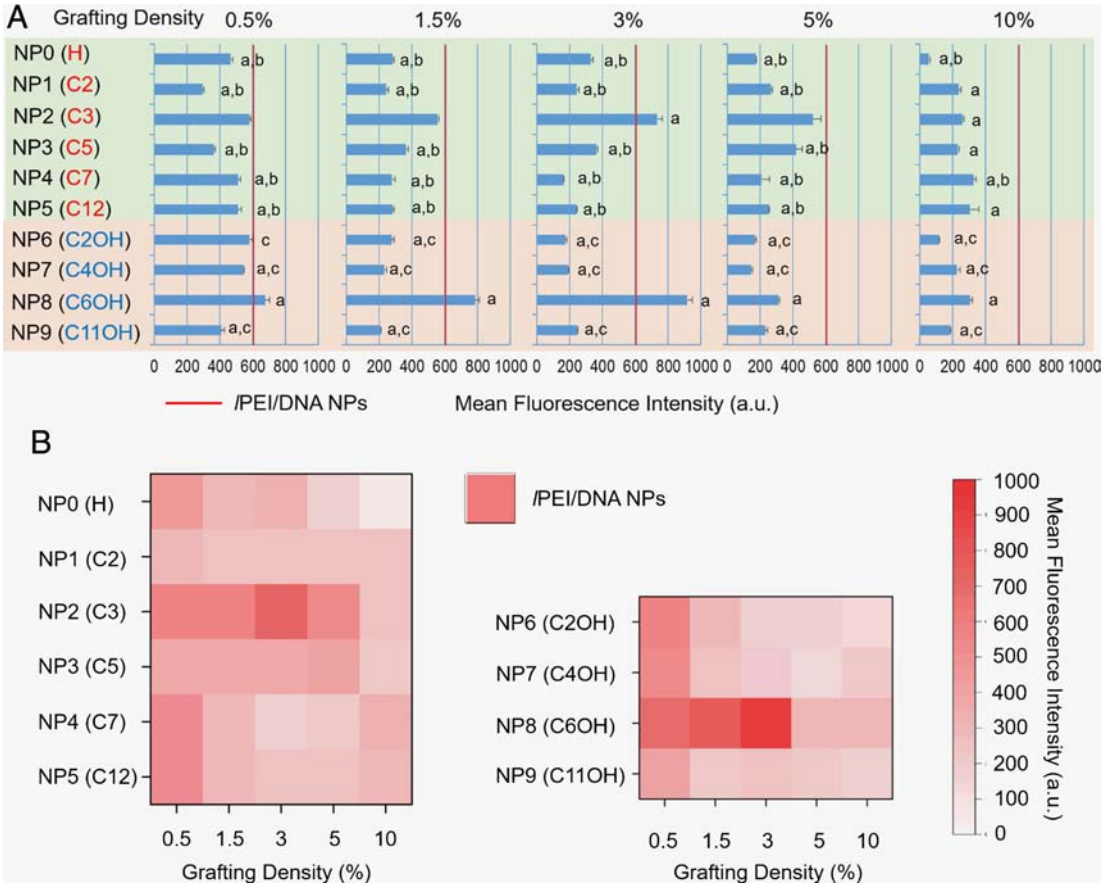

Figure 3. Cellular uptake levels of PEGylated DNA NPs with different PEG terminal groups in PC3 cells. **(A)** Bar charts showing the cellular uptake values of different NPs. *l*PEI/DNA NPs are used as control and their cellular uptake values are shown in red. a, $P < 0.05$, *vs.* *l*PEI/DNA NPs; b, $P < 0.05$, *vs.* NP2; c, $P < 0.05$, *vs.* NP8. **(B)** Heat maps comparing the cellular uptake levels of various NPs.

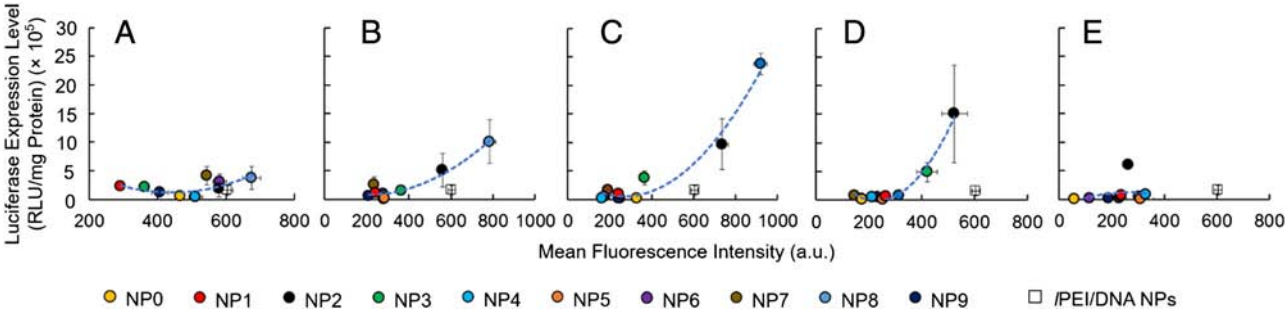

Figure 4. Relationship between transfection efficiency (luciferase expression level) and cellular uptake level (mean fluorescence intensity) of surface-functionalized DNA NPs at PEG grafting densities of 0.5% **(A)**, 1.5% **(B)**, 3% **(C)**, 5% **(D)**, and 10% **(E)**, respectively.

PEG grafting densities of 1.5 and 3% had higher stability than those formed by polymers at PEG grafting densities of 0.5, 5 and 10% (Figure S5A). This reflects two competing effects of PEG on the stability of PEGylated DNA NPs: protecting the *l*PEI/DNA core from the challenge of polyanions by forming a corona *vs.* weakening the electrostatic interactions between *l*PEI and DNA through steric hindrance.[13,23,24] At intermediate PEG grafting densities, where these two factors are balanced, these NPs show higher stability than all the other PEGylated NPs and *l*PEI/DNA NPs. All the polymers showed similar DNA binding abilities as unmodified PEI (Figure S5, *B*), indicating that short PEG grafts have a limited effect on DNA binding ability.

The last step in our preliminary evaluation concerns toxicity, which has been a limiting factor for the *in vivo* application of *l*PEI.[5] The toxicity of the polymers decreased with increasing of PEG grafting density (Figure S6), owing to the stealth property of PEG.[6] The high cell toxicity exhibited by NPs with intermediate alkyl chain lengths indicates that these NPs interact more strongly with cells than NPs with short or long alkyl chains.

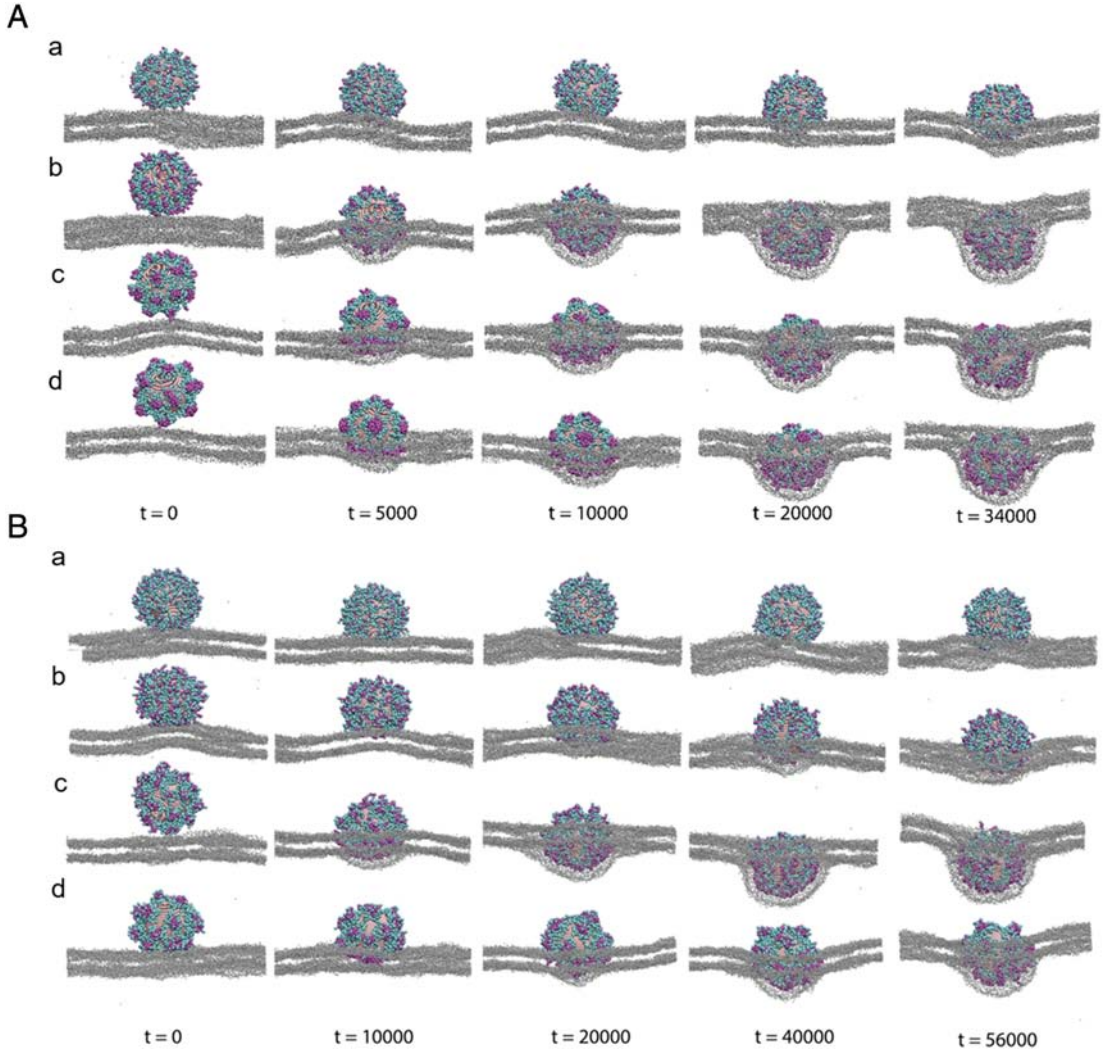

Figure 5. Evolution of the interaction between a lipid bilayer membrane and PEGylated NPs with various alkyl **(A)** or hydroxyalkyl **(B)** PEG terminal groups as a function of simulation time t (in reduced units τ, *cf.* Supplementary Information). The alkyl chains have lengths of 1 (a), 2 (b), 3 (c), or 4 (d) beads. Lipid tails groups and ions are not shown for clarity. Color codes: gray, lipid head; pink, NP core; cyan, hydrophilic PEG; purple, hydrophobic alkyl chain.

The transfection efficiency of various surface-functionalized DNA NPs was then evaluated in PC3 cells. Similar to our observations for the cytotoxicity (Figure S6), for each PEG grafting density optimal transfection efficiencies were achieved for intermediate alkyl chain lengths. The highest transfection levels were achieved by NP2 ($R = CH_3(CH_2)_2S–$) at PEG grafting density 5% and NP8 ($R = HO(CH_2)_6S–$) at PEG grafting density 3% for alkyl-decorated and hydroxyalkyl-decorated NPs respectively. PC3 cell viability after treatment with these NPs was 82% and 65%, respectively, higher than for *l*PEI/DNA NPs (55%, $P < 0.01$). This combination of high transfection efficiency and low toxicity shows that subtle changes in the PEG terminal groups can significantly improve the overall performance of PEGylated DNA NPs. Moreover, these functional changes can occur without changing the basic properties of the NPs. For example, at a PEG grafting density of 1.5%, NP2 ($R = CH_3(CH_2)_2S–$) showed 43-fold higher transfection efficiency than NP5 ($R = CH_3(CH_2)_{11}S–$) ($P < 0.01$), even though these two NPs had comparable size distribution, zeta potential, stability, and DNA binding ability.

As cellular uptake is one of the key steps significantly influencing transgene expression levels in cells,[3] we employ flow cytometry to quantify the cellular uptake levels of various *l*PEI-*g*-PEG-R/DNA NPs in PC3 cells and correlate them with the transfection efficiency. Similar with the trend found in transfection efficiency assay, NP2 and NP8 showed the highest cellular uptake levels in the two serials of NPs respectively at all PEG grafting densities (Figure 3). At PEG grafting densities of 1.5, 3 and 5%, positive correlations were found between transfection efficiency and cellular uptake level, while no correlation was found at PEG grafting densities of 0.5 and 10% (Figure 4). The discrepancies at PEG grafting densities of 0.5 and 10% may arise from other intracellular factors that affect the gene delivery efficiency, such as endosomal escape, DNA release, translocation of DNA to the nucleus, *etc.*[25,26]

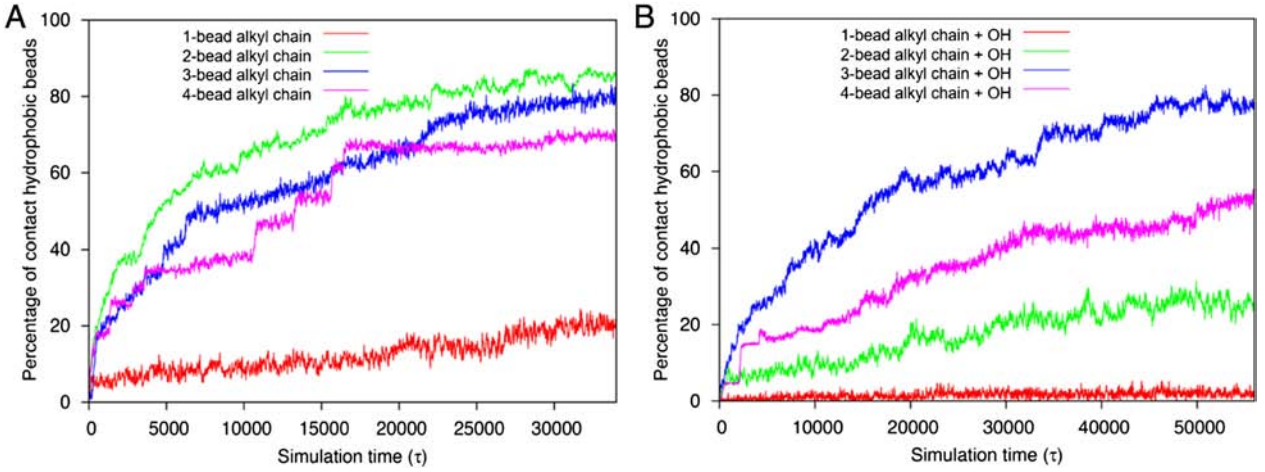

Figure 6. Percentage of hydrophobic beads on the surface of a NP in contact with the membrane as a function of simulation time during the interaction between the membrane and a PEGylated NP, for various alkyl **(A)** or hydroxyalkyl **(B)** PEG terminal groups.

When compared carriers with the same length of terminal alkyl chain and same grafting density but different end groups (hydroxyl *vs.* methyl group), the difference is striking. When the grafting density is between 1.5% and 10%, methyl end group favors the transfection activity and cellular uptake for shorter terminal chains (n = 2 and 4), as shown in Figure S8. The intermediate terminal chain (n = 6) yielded the highest differential activities between the two end groups. The ratio of transfection efficiencies of carrier with hydroxyl to that with methyl end group increased from 8.8 for PEG grafting density 0.5%, to 18 for 1.5%, to 116 for 3%, but then dropped drastically as the grafting density increased further ($r_{t.e.}$ = 1.5, at 5%; $r_{t.e.}$ = 0.6, at 10%). Interestingly, for longer chain (n = 11), higher $r_{t.e.}$ (7.2~8.9) occurred at higher grafting density (5 and 10%). Comparison in cellular uptake efficiency ($r_{c\cdot u.}$) between the two series of carriers did not show more than 3-fold of differences ($r_{c.u.}$ = 0.3-2.7), except for the one with an intermediate length (n = 6) and intermediate grafting density (3%). These analyses further confirm that grafting density and terminal group length are also critical parameters to consider when optimize the end group structure.

The confocal microscopy imaging showed similar results of the cellular uptake assay, with *l*PEI/DNA NPs and NP8 having much stronger fluorescence signal in the cells than NP5 and free DNA (Figure S7). In addition, strong signals were found inside the muclei of cells after being treated with NP8, while most signals were located in the cytosol in the lPEI/DNA NPs group. This indicates more rapid intracellular DNA release by NP8, contributing to its higher transfection efficiency (Figure 2).

To achieve a mechanistic understanding of the strong effect of alkyl chain length on cellular uptake, we employed MD simulations to probe the interactions between NPs and the cell membrane. As the large length scales of a gene delivery system preclude atomistic or even fine-level coarse-grained (CG) simulations (*e.g.*, using the Martini Force Field),[27] we resorted to more CG representations of the PEGylated DNA NPs and the cell membrane, with implicit solvent. The cell membrane was modeled as a bilayer of 4-bead long lipids with 6400 lipid molecules per layer. We introduced 10% negatively charged (−1 *e*) lipid head groups to reflect the slightly negative charge of biological membranes. In previous studies we showed that the complexation of plasmid DNA and PEG-grafted polycation leads to the formation of NPs with a polycation/DNA core and a neutral PEG corona.[28–30] The resulting NPs are typically overcharged, as shown in experiment (Figure S3) as well as simulations.[30] To reflect this, we employed a rigid spherical shell to represent the *l*PEI/DNA NP core and assume that ~70% of the core beads distributed on the surface of the shell are positively charged (+1 *e*). The PEG grafts along with their terminal groups were represented by a bead–spring model and directly bonded to these core beads to form the corona, with the PEG surface density chosen close to the estimated experimental grafting density of 3%. Whereas this model was too coarse-grained to precisely match the experimental system, it permitted qualitative reproduction of the observed trends and can provide insight into the possible underlying mechanisms of our experimental findings. We used 5 hydrophilic beads to represent each PEG graft and systematically vary the alkyl chain length from 1 to 4 hydrophobic beads. The hydroxyalkyl PEG terminal groups were represented by an additional hydrophilic bead at the end of each alkyl chain.

The simulation results showed that the NPs with intermediate alkyl chain length (2 beads for alkyl-decorated NPs and 3 beads for hydroxyalkyl-decorated NPs) had the most rapid engulfment by the cell membrane (Figure 5). We interpreted the engulfment of the NP as the first stage of endocytosis, so that the simulations suggest that PEG terminal groups with either alkyl chains that are either too short or too long will slow down the engulfment process. This phenomenon may contribute to the reduced cellular uptake efficiency observed in experiments (Figure 3). Moreover, the shift of the threshold to trigger engulfment for hydrophobic chains was qualitatively consistent with experiment, where the highest cellular uptake efficiency was observed at a chain length of 3 carbons for pure alkyl terminal groups *vs.* 6 carbons for hydroxyalkyl terminal groups.

The interaction between a surface-functionalized NP and the lipid membrane can be viewed as a two-step process:

electrostatically driven adhesion between the overcharged NP core and the negatively charged membrane, followed by hydrophobic contacts between the lipid tails and alkyl chains on the NP surface that lead to the rearrangement of PEG terminal groups and lipid molecules, in such a manner that more alkyl groups are exposed to the membrane tail region. For the NPs with the shortest pure alkyl chain length, due to the small energy gain induced by each alkyl chain insertion, the percentage of hydrophobic beads on the NP in contact with the lipid tails was less than 30% at the end of the simulation period (Figure 6, *A*). At longer alkyl chain length, the larger energy gain increased the retention probability of the inserted chain within the membrane. As a result, once more and more alkyl chains were inserted, the increasing hydrophobic contacts (Figure 6, *A*) provided enough energy to bend the membrane, gradually leading to a wrapped state of NPs. However, for even longer alkyl chain lengths, aggregation between the PEG terminal groups themselves resulted in the formation of hydrophobic patches at the surface of the NPs even before they interact with the membrane (Figure 5). These patches pose an additional barrier to the insertion of the alkyl chains. Whereas short alkyl chains were flexible and readily available to interact with the lipid membrane, longer alkyl chains aggregated in patches display reduced chain flexibility and face an energetic barrier to membrane insertion, slowing down the NP engulfment process.

When the alkyl chain modifications are terminated by a hydroxyl group, a similar mechanism occurred (Figure 5, *B* and Figure 6, *B*). Whereas pure alkyl terminal groups are able to insert entirely into the lipid membrane, the presence of the hydroxyl group constrains the arrangements of the PEG terminal groups with respect to the membrane. A typical configuration of the inserted chain is shown in Figure S9, where the hydroxyl terminal group remains located on the hydrophilic region of the membrane, while the alkyl chain is bent to maximize interaction with the membrane hydrophobic region. Thus, a longer alkyl chain was needed to provide sufficient attractive energy for bending and wrapping the NPs, as corroborated by the shift of engulfment threshold discussed above.

In these simulations, the thermodynamic driving force for NP engulfment was provided by the hydrophobic interactions between NP surface functional groups and lipid tails. In the experimental system, the full endocytosis process may also require the expenditure of ATP or the presence of membrane rafts, not taken into account in the MD simulations. Nevertheless, the simulations provided insight into the mechanistic role of PEG terminal groups with various alkyl chain lengths in PEGylated NP engulfment and consequently cellular uptake efficiency.

In summary, *via* an integrated experimental and computational approach we have uncovered the important role of PEG terminal groups in the interactions of PEGylated DNA NPs with cells. For PEGylated NPs modified with alkyl-chain terminal groups either with or without hydroxyl termination, we have demonstrated that the highest transfection efficiency and cellular uptake levels occur at intermediate alkyl chain length and intermediate PEG grafting density. The broader implication is that subtle changes in PEG terminal groups can significantly affect gene expression and cellular uptake levels. At PEG grafting densities ranging from of 1.5 to 5%, we found strong correlations between transfection efficiency and cellular uptake levels. The experimental observations were supported by MD simulations that demonstrated how NPs with intermediate alkyl chain lengths lead to the most rapid NP engulfment. These findings provide new insight and can serve as a guide toward future design of PEGylated NPs with optimized levels of cellular uptake and gene expression.

Appendix A. Supplementary data

Supplementary data to this article can be found online at https://doi.org/10.1016/j.nano.2019.04.004.

References

1. Yin H, Kanasty RL, Eltoukhy AA, Vegas AJ, Dorkin JR, Anderson DG. Non-viral vectors for gene-based therapy. *Nat Rev Genet* 2014;**15**:541-55.
2. Islam MA, Park TE, Singh B, Maharjan S, Firdous J, Cho MH, et al. Major degradable polycations as carriers for DNA and siRNA. *J Control Release* 2014;**193**:74-89.
3. Xia T, Kovochich M, Liong M, Meng H, Kabehie S, George S, et al. Polyethyleneimine coating enhances the cellular uptake of mesoporous silica nanoparticles and allows safe delivery of siRNA and DNA constructs. *ACS Nano* 2009;**3**:3273-86.
4. Jiang HL, Islam MA, Xing L, Firdous J, Cao W, He YJ, et al. Degradable polyethylenimine-based gene carriers for cancer therapy. *Top Curr Chem (Cham)* 2017;**375**:34.
5. Moghimi SM, Symonds P, Murray JC, Hunter AC, Debska G, Szewczyk A. A two-stage poly(ethylenimine)-mediated cytotoxicity: implications for gene transfer/therapy. *Mol Ther* 2005;**11**:990-5.
6. Williford JM, Archang MM, Minn I, Ren Y, Wo M, Vandermark J, et al. Critical length of PEG grafts on lPEI/DNA nanoparticles for efficient in vivo delivery. *ACS Biomater Sci Eng* 2016;**2**:567-78.
7. Bauhuber S, Liebl R, Tomasetti L, Rachel R, Goepferich A, Breunig M. A library of strictly linear poly(ethylene glycol)-poly(ethylene imine) diblock copolymers to perform structure-function relationship of non-viral gene carriers. *J Control Release* 2012;**162**:446-55.
8. Huang FW, Wang HY, Li C, Wang HF, Sun YX, Feng J, et al. PEGylated PEI-based biodegradable polymers as non-viral gene vectors. *Acta Biomater* 2010;**6**:4285-95.
9. Tang GP, Zeng JM, Gao SJ, Ma YX, Shi L, Li Y, et al. Polyethylene glycol modified polyethylenimine for improved CNS gene transfer: effects of PEGylation extent. *Biomaterials* 2003;**24**:2351-62.
10. Fitzsimmons RE, Uludag H. Specific effects of PEGylation on gene delivery efficacy of polyethylenimine: interplay between PEG substitution and N/P ratio. *Acta Biomater* 2012;**8**:3941-55.
11. Luo X, Feng M, Pan S, Wen Y, Zhang W, Wu C. Charge shielding effects on gene delivery of polyethylenimine/DNA complexes: PEGylation and phospholipid coating. *J Mater Sci Mater Med* 2012;**23**:1685-95.
12. Luo X, Pan S, Feng M, Wen Y, Zhang W. Stability of poly(ethylene glycol)-graft-polyethylenimine copolymer/DNA complexes: influences of PEG molecular weight and PEGylation degree. *J Mater Sci Mater Med* 2010;**21**:597-607.
13. Petersen H, Fechner PM, Martin AL, Kunath K, Stolnik S, Roberts CJ, et al. Polyethylenimine-graft-poly(ethylene glycol) copolymers: influence of copolymer block structure on DNA complexation and biological activities as gene delivery system. *Bioconjug Chem* 2002;**13**:845-54.
14. Williford JM, Ren Y, Liu HW, Mao HQ. *Surface functional groups of PEGylated DNA nanoparticles significantly impacts in vitro and in vivo delivery efficiency*; 2017. In prepration.

15. de Bruin K, Ruthardt N, von Gersdorff K, Bausinger R, Wagner E, Ogris M, et al. Cellular dynamics of EGF receptor-targeted synthetic viruses. *Mol Ther* 2007;**15**:1297-305.
16. Beh CW, Pan D, Lee J, Jiang X, Liu KJ, Mao HQ, et al. Direct interrogation of DNA content distribution in nanoparticles by a novel microfluidics-based single-particle analysis. *Nano Lett* 2014;**14**:4729-35.
17. Lindquist GM, Stratton RA. The role of polyelectrolyte charge density and molecular weight on the adsorption and flocculation of colloidal silica with polyethylenimine. *J Colloid Interface Sci* 1976;**55**:45-59.
18. Cooke IR, Deserno M. Solvent-free model for self-assembling fluid bilayer membranes: stabilization of the fluid phase based on broad attractive tail potentials. *J Chem Phys* 2005;**123**224710.
19. Lee MW, Han M, Bossa GV, Snell C, Song Z, Tang H, et al. Interactions between membranes and "metaphilic" polypeptide architectures with diverse side-chain populations. *ACS Nano* 2017;**11**:2858-71.
20. Rejman J, Oberle V, Zuhorn IS, Hoekstra D. Size-dependent internalization of particles via the pathways of clathrin- and caveolae-mediated endocytosis. *Biochem J* 2004;**377**:159-69.
21. Prabha S, Arya G, Chandra R, Ahmed B, Nimesh S. Effect of size on biological properties of nanoparticles employed in gene delivery. *Artif Cells Nanomed Biotechnol* 2016;**44**:83-91.
22. Navarro G, Pan J, Torchilin VP. Micelle-like nanoparticles as carriers for DNA and siRNA. *Mol Pharm* 2015;**12**:301-13.
23. Neu M, Germershaus O, Behe M, Kissel T. Bioreversibly crosslinked polyplexes of PEI and high molecular weight PEG show extended circulation times in vivo. *J Control Release* 2007;**124**:69-80.
24. Nimesh S, Goyal A, Pawar V, Jayaraman S, Kumar P, Chandra R, et al. Polyethylenimine nanoparticles as efficient transfecting agents for mammalian cells. *J Control Release* 2006;**110**:457-68.
25. Cai J, Yue Y, Wang Y, Jin Z, Jin F, Wu C. Quantitative study of effects of free cationic chains on gene transfection in different intracellular stages. *J Control Release* 2016;**238**:71-9.
26. Bishop CJ, Kozielski KL, Green JJ. Exploring the role of polymer structure on intracellular nucleic acid delivery via polymeric nanoparticles. *J Control Release* 2015;**219**:488-99.
27. Marrink SJ, Risselada HJ, Yefimov S, Tieleman DP, de Vries AH. The MARTINI force field: coarse grained model for biomolecular simulations. *J Phys Chem B* 2007;**111**:7812-24.
28. Jiang X, Qu W, Pan D, Ren Y, Williford JM, Cui H, et al. Plasmid-templated shape control of condensed DNA-block copolymer nanoparticles. *Adv Mater* 2013;**25**:227-32.
29. Wei Z, Ren Y, Williford JM, Qu W, Huang K, Ng S, et al. Simulation and experimental assembly of DNA–graft copolymer micelles with controlled morphology. *ACS Biomater Sci Eng* 2015;**1**:448-55.
30. Wei Z, Luijten E. Systematic coarse-grained modeling of complexation between small interfering RNA and polycations. *J Chem Phys* 2015;**143**243146.